

Article

Powder Pressed Cuprous Iodide (CuI) as A Hole Transporting Material for Perovskite Solar Cells

Siva Uthayaraj ^{1,2}, D. G. B. C. Karunaratne ³, G. R. A. Kumara ³,
Thanihachelvan Murugathas ¹, Shivatharsiny Rasalingam ⁴, R. M. G. Rajapakse ⁵,
Punniamoorthy Ravirajan ^{1,*} and Dhayalan Velauthapillai ^{2,*}

¹ Department of Physics, University of Jaffna, Jaffna 40000, Sri Lanka

² Faculty of Engineering and Science, Western Norway University of Applied Sciences, P.O. Box 7030, 5020 Bergen, Norway

³ National Institute of Fundamental Studies, Hantana Road, Kandy 20000, Sri Lanka

⁴ Department of Chemistry, University of Jaffna, Jaffna 40000, Sri Lanka

⁵ Department of Chemistry, Faculty of Science, University of Peradeniya, Peradeniya 20400, Sri Lanka

* Correspondence: pravirajan@gmail.com (P.R.); Dhayalan.Velauthapillai@hvl.no (D.V.);
Tel.: +94-21-222-5924 (P.R.); +47-55-587711 (D.V.)

Received: 27 May 2019; Accepted: 25 June 2019; Published: 26 June 2019



Abstract: This study focuses on employing cuprous iodide (CuI) as a hole-transporting material (HTM) in fabricating highly efficient perovskite solar cells (PSCs). The PSCs were made in air with either CuI or 2,2',7,7'-Tetrakis[N,N-di(4-methoxyphenyl)amino]-9,9'-spirobifluorene (spiro-OMeTAD) as HTMs. A simple and novel pressing method was employed for incorporating CuI powder layer between perovskite layer and Pt top-contact to fabricate devices with CuI, while spiro-OMeTAD was spin-coated between perovskite layer and thermally evaporated Au top-contact to fabricate devices with spiro-OMeTAD. Under illuminations of 100 mW/cm² with an air mass (AM) 1.5 filter in air, the average short-circuit current density (J_{SC}) of the CuI devices was over 24 mA/cm², which is marginally higher than that of spiro-OMeTAD devices. Higher J_{SC} of the CuI devices can be attributed to high hole-mobility of CuI that minimizes the electron-hole recombination. However, the average power conversion efficiency (PCE) of the CuI devices were lower than that of spiro-OMeTAD devices due to slightly lower open-circuit voltage (V_{OC}) and fill factor (FF). This is probably due to surface roughness of CuI powder. However, optimized devices with solvent-free powder pressed CuI as HTM show a promising efficiency of over 8.0 % under illuminations of 1 sun (100 mW/cm²) with an air mass 1.5 filter in air, which is the highest among the reported efficiency values for PSCs fabricated in an open environment with CuI as HTM.

Keywords: perovskite solar cells; hole-transporting material; powder pressing; cuprous iodide; CuI; spiro-OMeTAD; air stable

1. Introduction

Perovskite solar cells based on methylammonium lead halides perovskite material with spiro-OMeTAD as hole-collector have attracted considerable attention of research and industrial community due to the rapid growth of efficiency from 3.8% to 24.2% [1–5] in recent years. However, spiro-OMeTAD in its pristine form still shows some intrinsic drawbacks, such as relatively low hole mobility and conductivity, as well as it is a highly expensive material and it needs dopants [6]. As such, replacing this hole-collector by a low-cost, dopant-free alternative would result in bringing down the overall cost of the device. Several works have been reported on use of cuprous iodide (CuI) as hole transporting material in place of liquid electrolyte in Grätzel type of solar cells [7–11] as CuI possesses

several unique characteristics, such as high transparency, low-production cost, ease of deposition, high hole-mobility, and good chemical stability [12]. With the help of crystal growth inhibitor triethylammonium thiocyanate, over 5.0% efficiency was achieved for all solid-state dye-sensitized solar cells based on CuI HTMs [13,14]. Christians et al. reported the best efficiency of 6.0% with the perovskite solar cell based on CuI HTM ($J_{SC} = 17.8 \text{ mA/cm}^2$, $V_{OC} = 0.55 \text{ V}$ and $FF = 0.62$) [15]. In these studies, CuI was chemically deposited using di-n-propyl sulfide and chlorobenzene. Qin et al. used solution processed cuprous thiocyanate (CuSCN) as HTM in perovskite solar cell and obtained an impressive efficiency of over 12.4% [16] under 1 Sun illumination. Huangfu et al. obtained 5.8% efficiency in the perovskite solar cell with spray coated CuI as the HTM [17]. Hu et al. were able to obtain 9.12% efficiency by modifying the photoanode to have TiO₂ nanotube/TiO₂ nanoparticle hybrid structure [18] with spray coated CuI. Sepalage et al. obtained an efficiency of 7.5% for perovskite solar cell based on CuI hole transporting material, where the CuI layer was deposited by doctor blading method [19].

CuI has several important properties contributing to its application as an HTM in perovskite solar cells [20]. Takahashi and Suzuki reported that valence band edge of chemically stable CuI is very close to highest occupied molecular orbital (HOMO) level of widely studied spiro-OMeTAD (5.2 eV) hole-transporting materials for PSCs [21–23]. Hole mobilities in spiro-OMeTAD and CuI are $\sim 2 \times 10^{-4} \text{ cm}^2\text{V}^{-1}\text{s}^{-1}$ and $43.9 \text{ cm}^2\text{V}^{-1}\text{s}^{-1}$ respectively [24–27], which means that the hole mobility of CuI is over 10^5 -fold higher than that of spiro-OMeTAD. CuI thin films can be deposited at low temperature [28] and this film is a p-type semiconductor with a relatively wide band gap of 3.1 eV. Moreover, the cost of CuI is over 10-fold less than that of spiro-OMeTAD, and it can readily be deposited on perovskite film for large scale production of perovskite solar modules. Although CuI seems to have such a vast advantage over spiro-OMeTAD and various techniques have already been adopted for deposition of CuI [3,29] in fabricating PSCs, the highest efficiency values reported for CuI devices is 10% which is 2.2 times lower than that of spiro-OMeTAD devices [30] under a controlled environment. In this reported work [30], a mixed solvent system comprising of chlorobenzene, acetonitrile, and 4-tert-Butylpyridine in 40:20:1 volume ratio has been used, since the pure acetonitrile solvent dissolves the perovskite layer. However, chlorobenzene is a solvent categorized as a toxic substance which has shown acute and intermediate exposure in animals tend to cause narcosis, restlessness, tremors and muscle spasms.

This work attempted to fabricate solvent-free route to make CuI hole-transporting materials by simply pressing CuI between perovskite layer and Pt-coated FTO glass. All the fabrication and characterization processes were carried out in air. This solvent-free pressed method of hole transport material is hazard free and simple method capable for the large-scale production of PSCs. For comparison purpose, PSCs were fabricated by spin-coating spiro-OMeTAD between perovskite layer and thermally evaporated Au top-contact under the same open environment.

2. Materials and Methods

2.1. Materials

Fluorine-doped Tin Oxide (FTO, surface resistivity of $10 \Omega/\text{square}$), Methylammonium Iodide (MAI, 98%), Lead (II) Chloride (98%), N,N-Dimethylformamide, (DMF, Anhydrous 99.8%), 2,2',7,7'-Tetrakis[N,N-di(4-methoxyphenyl)amino]-9,9'-spirobifluorene, spiro-OMeTAD (99%), Chlorobenzene (Anhydrous 99.8%), Bis(trifluoromethane) sulfonamide lithium salt (Li-TFSI, 99.95%), 4-tert-Butylpyridine (96%), Acetonitrile (99.8%), Cuprous Iodide (CuI, 98%), Titanium di-isopropoxide bis (acetylacetonate) 75% (w/w), Ethanol (absolute, for HPLC, $\geq 99.8\%$) and poly(3-hexylthiophene-2,5-diyl) were purchased from Sigma-Aldrich (Oslo, Norway). 18NR-T Transparent Titania Paste was purchased from Great Cell Solar (Queanbeyan, Australia). All solvents were used without any further purification.

2.2. Solar Cell Fabrication

FTO substrates were cleaned with detergent for 20 min. and then with distilled water for 20 min. and finally, with ethanol for 20 min. in an ultrasonic bath. A dense layer and porous layer of TiO₂ was deposited by spray and spin coating as reported elsewhere [31–34]. A dense layer precursor solution was prepared by mixing 700 µL of titanium diisopropoxide bis(acetylacetonate) in 7.0 mL of absolute ethanol and filtering through 0.2 µm pore syringe filter. 3.3 mL of the above solution was sprayed at 400 °C on to the cleaned FTO surface over a period of 10 min. and then annealed at 500 °C in a furnace for 10 min. It was then allowed to cool down to room temperature and ultra-sonicated in absolute ethanol for 20 min. The porous TiO₂ thin film was deposited on the dense layer by spin coating a mixture of TiO₂ paste (18 NR-T Dysol) and ethanol in 2:7 weight ratio (w/w) at 4500 rpm for 30 s. It was then calcinated at 450 °C for 30 min. The perovskite precursor solution was prepared by dissolving methylammonium iodide and lead (II) chloride in 3:1 molar ratio in 700 µL of DMF and stirring for 1 hr at 70 °C. This suspension was then spin coated onto the TiO₂ porous layer at 2000 rpm for 30 s [35]. It was then sintered at 120 °C for 45 min. Then, selected HTMs were deposited by the following methods:

2.2.1. CuI Powder Pressing

Fine powder of CuI (98%, grain size of 0.2 µm) was spread onto the perovskite surface and the cell was completed by pressing it with Pt - counter electrode (made by sputtering process on FTO glass) as shown in the Figure 1.

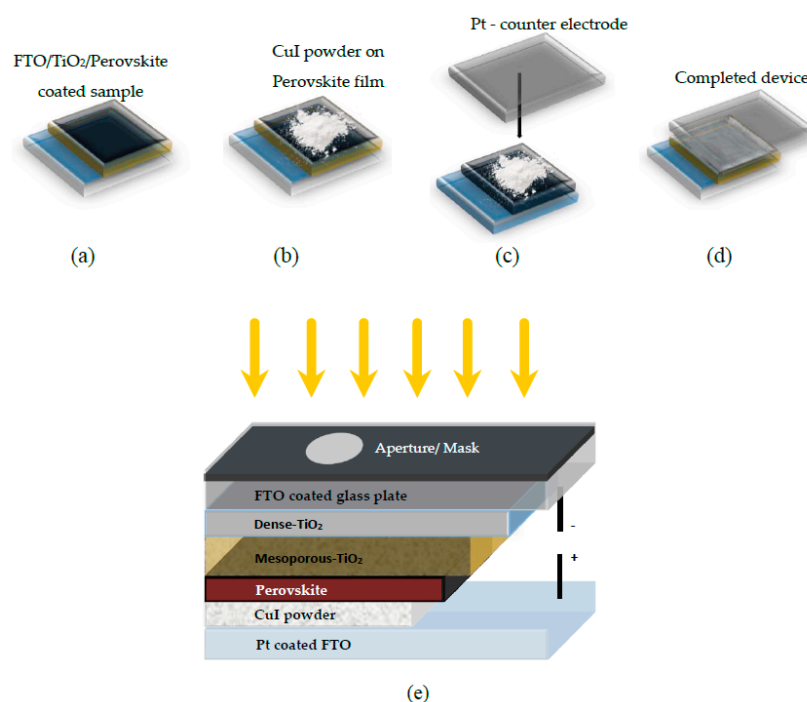


Figure 1. (a–d) step by step schematic of powder pressing method for incorporating cuprous iodide (CuI) powder as HTM in perovskite solar cells (PSCs) and (e) schematic representation of CuI device architecture.

2.2.2. Deposition of Spiro-OMeTAD

1 mL of 97 mg/mL spiro-OMeTAD in chlorobenzene mixed with 30.2 µL of 175 mg/mL Bis(trifluoromethane) sulfonamide lithium salt in acetonitrile and 9.7 µL of solution consists of 46.6% of 4-tert-butylpyridine in acetonitrile. This mixed solution was spin coated on the perovskite film at 2000 rpm for 30 s [35]. Finally, 80 nm Au electrode was deposited on spiro-OMeTAD coated

devices by thermal evaporation at a constant evaporation rate of 0.2 \AA/s under 1×10^{-6} torr vacuum. Except for thermal evaporation, all the device fabrications were carried out in air. Figure 1e shows a schematic representation of CuI device architecture.

2.3. Electrical Characterization

The photovoltaic performance of fabricated PSCs was measured by using a computer controlled Keithley 2400 source meter (Cleveland, OH, USA) with a delay time of 50 ms under illuminations of 100 mW/cm^2 (1 sun) with air mass (AM) 1.5 filter, with a solar simulator (Pecell-PEC-L12, Kanagawa, Japan). The solar simulator was calibrated using standard Silicon photodiode. The active area of the cell was 4.2 mm^2 . All samples were measured in air at room temperature.

2.4. Structural Characterization

The crystalline structure and phase purity of CuI powder were analyzed using X-ray diffraction spectroscopy (XRD, PANalytical-AERIS, Almelo, The Netherland). The diffraction pattern was collected with Cu $K\alpha$ radiation ($\lambda = 1.5408 \text{ \AA}$) at ambient temperature, under the following operating conditions; accelerating voltage of 40 kV; emission current of 44 mA; scanned range (2θ) between 10° and 90° with a step size of 0.0027° and a scan speed of $4^\circ/\text{min}$.

3. Results and Discussion

Firstly, CuI powder was characterized using XRD. Figure 2 shows the XRD pattern of as-received CuI powder, in which the grain size of 0.2 \mu m . The CuI powder exhibits major diffraction peaks at 2θ values of 25.43° , 29.45° , 42.15° , 49.88° , 67.34° , and 77.09° correspond to (111), (200), (220), (311), (331) and (422) planes, respectively. These are in good agreement with the structure of γ -CuI (JCPDS Card No. 06-0246) [20,36]. The higher peaks at 25.43° show that the orientation of γ -CuI is (111) preference [37]. However, a few additional peaks were also observed in the XRD pattern, which could be attributed to the fact of the reaction of CuI in air, moisture, and impurities.

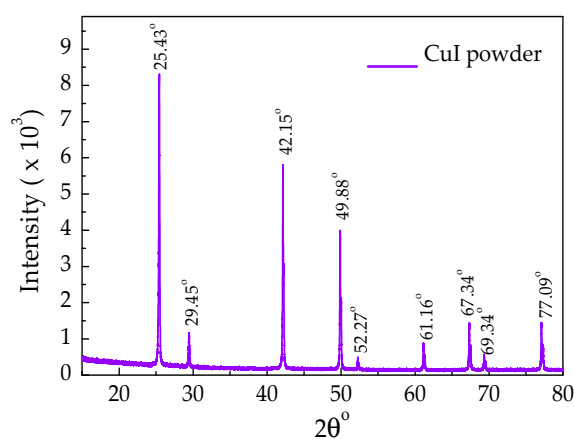


Figure 2. XRD spectra of Cuprous Iodide powder.

Then the opto-electronic properties of the fabricated PSCs were examined under 100 mW/cm^2 , AM 1.5 simulated solar irradiation (1 sun). The J-V characteristic of the best (champion) devices with spiro-OMeTAD and CuI as the HTM are shown in Figure 3. Table 1 summarizes the average photovoltaic properties of six solar cells fabricated with each of two hole-conducting material along with the performance of the champion cell. It is clear that the PV performance of the devices with spiro-OMeTAD as the HTM outperformed the CuI devices. As discussed in the literature, the spiro-OMeTAD is shown to be the best HTM for PSCs so far. However, it can be noted that the J_{SC} of the devices with CuI is marginally higher than that of the spiro devices fabricated under ideal conditions. As in Table 1, the average J_{SC} of the CuI devices was $24.09 \pm 1.4 \text{ mA/cm}^2$ which is higher

than that of spiro-OMeTAD devices (22.4 ± 1.7 mA/cm²). This is consistent with higher hole-mobility found in CuI than spiro-OMeTAD to CuI [38]. The efficient charge extraction between the perovskite and CuI lead to an excellent hole injection from the active perovskite films to CuI layer [39].

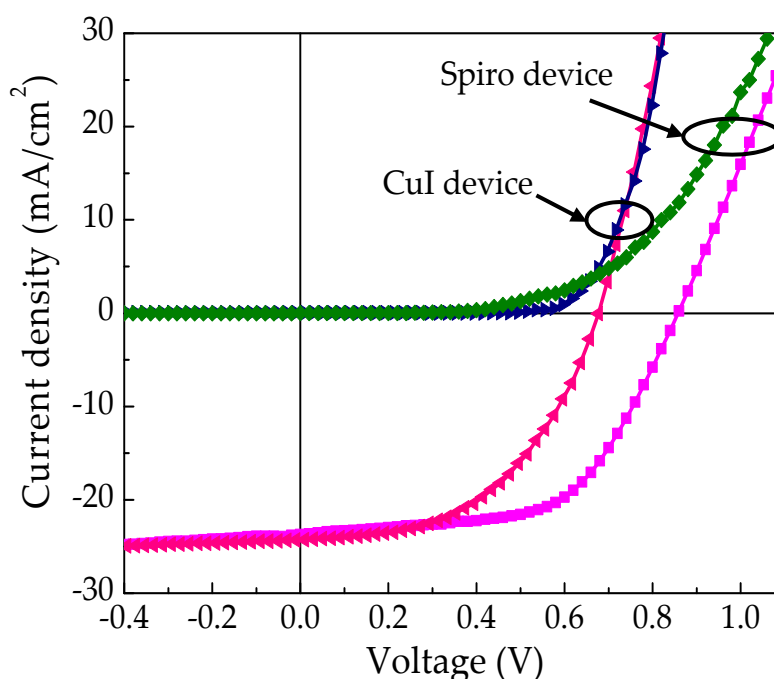


Figure 3. J-V characteristic of champion FTO/TiO₂/MAPbI_xCl_{3-x}/CuI/Pt and FTO/TiO₂/MAPbI_xCl_{3-x}/spiro-OMeTAD/Au devices under illuminations of 100 mW/cm² (1 sun) with air mass (AM) 1.5 filter and in dark.

Table 1. The variation of photovoltaic parameters for the different HTM devices under illuminations of 100 mW/cm² (1 sun) with air mass (AM) 1.5 filter. (The values in bold text are from the champion cell).

Hole Transporting Material (HTM)	J _{SC} (mA/cm ²)	V _{OC} (V)	FF	PCE (η%)
Spiro-OMeTAD	22.4 ± 1.7	0.79 ± 0.03	0.56 ± 0.07	9.9 ± 1.3
	23.7	0.85	0.59	11.9
CuI	24.09 ± 1.4	0.66 ± 0.02	0.49 ± 0.03	7.8 ± 0.3
	24.23	0.67	0.50	8.1

However, the performance of the devices with CuI as HTMs was limited with lower V_{OC} (0.66 ± 0.02 V) and FF (0.49 ± 0.03) than that of the devices with spiro-OMeTAD (V_{OC} = 0.79 ± 0.03 V and FF = 0.56 ± 0.07) as HTMs. The lower fill factor of the CuI devices can be correlated to the higher thickness and roughness of the pressed CuI layer. Thickness of the CuI layer should be optimized to further enhance the efficiency of the cells [40]. According to our experience, controlling the thickness (~1 nm) of the CuI layer by using the pressing method is quite challenging. The average V_{OC} of the CuI based PSCs, were 0.66 ± 0.02 V, which is lower than spiro-OMeTAD based PSCs, that we tested under the same conditions. The lower V_{OC} of CuI devices can be attributed to an increase in recombination rate, which is due to induced valance band trap states caused by free iodine ions in the CuI [15]. It should be noted that the spiro-OMeTAD devices fabricated in our laboratory have efficiencies lower than that of reported spiro-OMeTAD devices in a closed environment [41]. In our work, all the device fabrication process and characterizations were done in an open atmosphere. This could be the reason for the lower performance of the devices.

Figure 4 illustrates the proposed energy band diagram of fabricated PSCs in our work. The energies are expressed in electron volts (eV), using the electron energy in a vacuum as the reference.

The conduction band (CB) of TiO_2 and $\text{CH}_3\text{NH}_3\text{PbI}_x\text{Cl}_{3-x}$ are at -4.1 eV and -3.7 eV, respectively. Whereas, the edge of the valance band (VB) of $\text{CH}_3\text{NH}_3\text{PbI}_x\text{Cl}_{3-x}$ and CuI are at -5.4 eV and -5.1 eV respectively. The spiro-OMeTAD has HOMO levels around -5.2 eV [42–45]. It is well-known that the selection of HTMs on the device architectures and device fabrication process affects the PV performance of the devices [46]. Device characteristics of PSCs reported in the literature with CuI as HTMs employing different techniques are listed in Table 2. Here we note that the selected HTMs, CuI and spiro-OMeTAD have similar levels for hole transport and the changes in the performance of the devices may be attributed to different hole mobilities of CuI and spiro-OMeTAD.

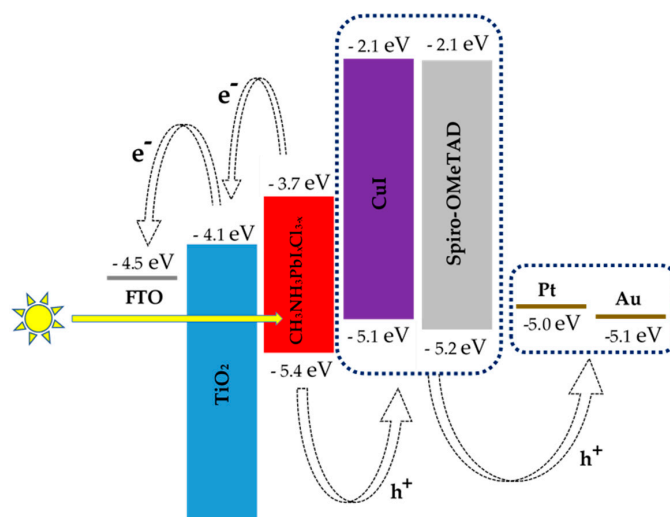


Figure 4. Proposed energy band diagram for the fabricated PSCs.

Table 2. Comparison of perovskite solar cells (PSCs) reported in the literature with CuI as the hole transporting material fabricated by different techniques.

Device Structure	CuI Deposition Method	J_{sc} (mA/cm ²)	V_{oc} (V)	FF	PCE (η %)	Reference
$\text{TiO}_2/\text{CH}_3\text{NH}_3\text{PbI}_3/\text{CuI}$	Solution pumping process	17.8	0.55	0.62	6.0	[15]
$\text{TiO}_2/\text{CH}_3\text{NH}_3\text{PbI}_x\text{Cl}_{3-x}/\text{CuI}$	Spray coating method	22.3	0.61	0.42	5.8	[17]
$\text{TiO}_2/\text{CH}_3\text{NH}_3\text{PbI}_3/\text{CuI}$	Spin coating method	14.7	0.42	0.40	2.2	[47]
$\text{TiO}_2/\text{CH}_3\text{NH}_3\text{PbI}_3/\text{CuI}$	Doctor blading method	16.7	0.78	0.57	7.5	[19]
$\text{TiO}_2/\text{CH}_3\text{NH}_3\text{PbI}_3/\text{CuI}$	Gas-solid treatment	32.7	0.73	0.31	7.4	[22]
$\text{CuI}/\text{CH}_3\text{NH}_3\text{PbI}_3/\text{PCBM}$	Doctor blading method	12.3	0.57	0.47	3.4	[48]
$\text{CuI}/\text{CsSnI}_3/\text{C}_{60}/\text{BCP}$	Thermal evaporation	8.94	0.36	0.54	2.1	[23]
$\text{TiO}_2/\text{CH}_3\text{NH}_3\text{PbI}_3/\text{CuI}/\text{Cu}$	Thermal evaporation	23.0	0.85	0.47	9.2	[30]
$\text{TiO}_2/\text{CH}_3\text{NH}_3\text{PbI}_x\text{Cl}_{3-x}/\text{CuI}$	Powder pressing method	24.23	0.67	0.50	8.1	This work

As listed in Table 2, except thermally evaporated CuI/Cu based PSCs, the average PCE of our device is the highest among the reported works on CuI as HTM for PSCs. However, V_{oc} and FF are slightly lower than that of reported works. This may be due to the high level of porosity in the CuI layer fabricated using the pressing method compared to other methods such as spin coating, spray coating, evaporation method, etc. This limits the PCE of CuI based devices due to air voids and the trapping effect of charge carriers. This study reveals that the pressing method is a facile, hazard free and cost-effective method, which can be employed effectively for PSCs with CuI as HTM.

4. Conclusions

In this study, the focus has been on replacing the highly expensive spiro-OMeTAD that is used as hole transporting material in perovskite solar cells with a low-cost, dopant-free alternative. The study has resulted in successful fabrication of efficient PSCs with CuI hole transporting material employing a novel and simple powder pressing method. A variety of $\text{FTO}/\text{TiO}_2/\text{MAPbI}_x\text{Cl}_{3-x}/\text{CuI}/\text{Pt}$ and

FTO/TiO₂/MAPbI_xCl_{3-x}/spiro-OMeTAD/Au are fabricated and the champion devices are compared. A powder pressed CuI offers J_{SC} over 24 mA/cm², V_{OC} of 0.67 V, fill factor of 0.50, which yields promising efficiency of 8.1% in air for the PSC. Although spiro-OMeTAD based PSC had higher V_{OC} and FF, powder pressed CuI had higher J_{SC}. Promising efficiencies obtained with a simple pressing method of CuI in an open environment shows the high potential of CuI as hole transporting material in PSCs.

Author Contributions: Conceptualization, P.R., G.R.A.K., S.R., R.M.G.R. and D.V.; methodology, S.U., G.R.A.K. and S.R.; analysis, S.U., P.R., D.G.B.C.K., G.R.A.K., S.R., R.M.G.R., T.M., and D.V.; investigation, P.R., G.R.A.K., S.R., R.M.G.R., T.M., and D.V.; resources, P.R., G.R.A.K., R.M.G.R. and D.V.; data curation, S.U., S.R., T.M., P.R. and D.V.; writing—original draft preparation, S.U. and T.M.; writing—review and editing, P.R., G.R.A.K., S.R., R.M.G.R., T.M., and D.V.; supervision, P.R., G.R.A.K., S.R., R.M.G.R. and D.V.; project administration and funding acquisition, P.R. and D.V.

Funding: This research was funded by Capacity Building and Establishment of a Research Consortium (CBERC) project, grant number LKA-3182-HRNCET and Higher Education and Research collaboration on Nanomaterials for Clean Energy Technologies (HRNCET) project, grant number NORPART/2016/10237.

Conflicts of Interest: The authors declare no conflict of interest. The funders had no role in the design of the study; in the collection, analyses, or interpretation of data; in the writing of the manuscript, or in the decision to publish the results

References

- Juarez-Perez, E.J.; Wang, S.; Ono, L.K.; Qi, Y.; Leyden, M.R.; Hawash, Z. Role of the Dopants on the Morphological and Transport Properties of Spiro-MeOTAD Hole Transport Layer. *Chem. Mater.* **2016**, *28*, 5702–5709. [[CrossRef](#)]
- Jung, H.S.; Park, N.G. Perovskite solar cells: From materials to devices. *Small* **2015**, *11*, 10–25. [[CrossRef](#)]
- Velauthapillai, D.; Rangasamy, B.; Natarajan, M.; Santhanam, A.; Selvaraj, Y.; Asokan, V.; Sundaram, S.; Yuvapragasam, A.; Madurai Ramakrishnan, V.; Pitchaiya, S. The Performance of CH₃NH₃PbI₃ - Nanoparticles based – Perovskite Solar Cells Fabricated by Facile Powder press Technique. *Mater. Res. Bull.* **2018**, *108*, 61–72.
- Zhou, H.; Shi, Y.; Dong, Q.; Zhang, H.; Xing, Y.; Wang, K.; Du, Y.; Ma, T. Hole-Conductor-Free, Metal-Electrode-Free TiO₂/CH₃NH₃PbI₃ Heterojunction Solar Cells Based on a Low-Temperature Carbon Electrode. *J. Phys. Chem. Lett.* **2014**, 3241–3246. [[CrossRef](#)]
- Cheng, Y.; So, F.; Tsang, S.-W. Progress in air-processed perovskite solar cells: from crystallization to photovoltaic performance. *Mater. Horizons* **2019**. [[CrossRef](#)]
- Hua, Y.; Liu, P.; Li, Y.; Sun, L.; Kloo, L. Composite Hole-Transport Materials Based on a Metal-Organic Copper Complex and Spiro-OMeTAD for Efficient Perovskite Solar Cells. *Sol. RRL* **2018**, *2*, 1700073. [[CrossRef](#)]
- Kumara, G.R.A.; Konno, A.; Shiratsuchi, K.; Tsukahara, J.; Tennakone, K. Dye-sensitized solid-state solar cells: Use of crystal growth inhibitors for deposition of the hole collector. *Chem. Mater.* **2002**, *14*, 954–955. [[CrossRef](#)]
- Tennakone, K.; Kumara, G.R.R.A.; Kottegoda, I.R.M.; Wijayantha, K.G.U.; Perera, V.P.S. A solid-state photovoltaic cell sensitized with a ruthenium bipyridyl complex. *J. Phys. D. Appl. Phys.* **1998**, *31*, 1492–1496. [[CrossRef](#)]
- Tennakone, K.; Kumara, G.R.R.A.; Kottegoda, I.R.M.; Wijayantha, K.G.U. The photostability of dye-sensitized solid state photovoltaic cells: Factors determining the stability of the pigment in a nanoporous n-TiO₂/cyanidin/p-CuI cell. *Semicond. Sci. Technol.* **1997**, *12*, 128–132. [[CrossRef](#)]
- Tennakone, K.; Kumara, G.R.R.A.; Wijayantha, K.G.U. The suppression of the recombination of photogenerated carriers in a dye-sensitized nano-porous solid-state photovoltaic cell. *Semicond. Sci. Technol.* **1996**, *11*, 1737–1739. [[CrossRef](#)]
- Search, H.; Journals, C.; Contact, A.; Iopscience, M.; Address, I.P. A dye-sensitized nano-porous solid-state photovoltaic cell. *Semicond. Sci. Technol.* **1995**, *10*, 1689.
- Yamada, N.; Ino, R.; Ninomiya, Y. Truly Transparent p-Type γ -CuI Thin Films with High Hole Mobility. *Chem. Mater.* **2016**, *28*, 4971–4981. [[CrossRef](#)]

13. Kumara, G.R.A.; Okuya, M.; Murakami, K.; Kaneko, S.; Jayaweera, V.V.; Tennakone, K. Dye-sensitized solid-state solar cells made from magnesiumoxide-coated nanocrystalline titanium dioxide films: Enhancement of the efficiency. *J. Photochem. Photobiol. A Chem.* **2004**, *164*, 183–185. [[CrossRef](#)]
14. Kumara, G.R.A.; Kaneko, S.; Okuya, M.; Tennakone, K. Fabrication of Dye-Sensitized Solar Cells Using Triethylamine Hydrothiocyanate as a CuI Crystal Growth Inhibitor. *Langmuir* **2002**, *18*, 10493–10495. [[CrossRef](#)]
15. Christians, J.A.; Fung, R.C.M.; Kamat, P.V. An inorganic hole conductor for Organo-lead halide perovskite solar cells. improved hole conductivity with copper iodide. *J. Am. Chem. Soc.* **2014**, *136*, 758–764. [[CrossRef](#)] [[PubMed](#)]
16. Tetreault, N.; Nazeeruddin, M.K.; Tanaka, S.; Grätzel, M.; Qin, P.; Ito, S.; Manabe, K.; Nishino, H. Inorganic hole conductor-based lead halide perovskite solar cells with 12.4% conversion efficiency. *Nat. Commun.* **2014**, *5*, 1–6.
17. Huangfu, M.; Shen, Y.; Zhu, G.; Xu, K.; Cao, M.; Gu, F.; Wang, L. Copper iodide as inorganic hole conductor for perovskite solar cells with different thickness of mesoporous layer and hole transport layer. *Appl. Surf. Sci.* **2015**, *357*, 2234–2240. [[CrossRef](#)]
18. Qin, T.; Lv, S.; Yu, Y.; Zhang, J.; Liu, Z.; Wei, F.; Xu, H.; Cui, G.; Pang, S.; Hu, H. NH₂CH=NH₂PbI₃: An Alternative Organolead Iodide Perovskite Sensitizer for Mesoscopic Solar Cells. *Chem. Mater.* **2014**, *26*, 1485–1491.
19. Sepalage, G.A.; Meyer, S.; Pascoe, A.; Scully, A.D.; Huang, F.; Bach, U.; Cheng, Y.B.; Spiccia, L. Copper(I) Iodide as Hole-Conductor in Planar Perovskite Solar Cells: Probing the Origin of J-V Hysteresis. *Adv. Funct. Mater.* **2015**, *25*, 5650–5661. [[CrossRef](#)]
20. Kokubun, Y.; Watanabe, H.; Wada, M. Electrical Properties of CuI Thin Films. *Jpn. J. Appl. Phys.* **1971**, *10*, 864. [[CrossRef](#)]
21. Wang, H.; Yu, Z.; Jiang, X.; Li, J.; Cai, B.; Yang, X.; Sun, L. Efficient and Stable Inverted Planar Perovskite Solar Cells Employing CuI as Hole-Transporting Layer Prepared by Solid–Gas Transformation. *Energy Technol.* **2017**, *5*, 1836–1843. [[CrossRef](#)]
22. Gharibzadeh, S.; Nejand, B.A.; Moshaii, A.; Mohammadian, N.; Alizadeh, A.H.; Mohammadpour, R.; Ahmadi, V.; Alizadeh, A. Two-step physical deposition of a compact cui hole-transport layer and the formation of an interfacial species in perovskite solar cells. *ChemSusChem* **2016**, *9*, 1929–1937. [[CrossRef](#)] [[PubMed](#)]
23. Marshall, K.P.; Walton, R.I.; Hatton, R.A. Tin perovskite/fullerene planar layer photovoltaics: Improving the efficiency and stability of lead-free devices. *J. Mater. Chem. A* **2015**, *3*, 11631–11640. [[CrossRef](#)]
24. Chen, D.; Wang, Y.; Lin, Z.; Huang, J.; Chen, X.; Pan, D.; Huang, F. Growth strategy and physical properties of the high mobility p-type cui crystal. *Cryst. Growth Des.* **2010**, *10*, 2057–2060. [[CrossRef](#)]
25. Li, M.H.; Hsu, C.W.; Shen, P.S.; Cheng, H.M.; Chi, Y.; Chen, P.; Guo, T.F. Novel spiro-based hole transporting materials for efficient perovskite solar cells. *Chem. Commun.* **2015**, *51*, 15518–15521. [[CrossRef](#)] [[PubMed](#)]
26. Poplavskyy, D.; Nelson, J. Nondispersive hole transport in amorphous films of methoxy-spirofluorene-arylamine organic compound. *J. Appl. Phys.* **2003**, *93*, 341–346. [[CrossRef](#)]
27. Schmidt-Mende, L.; Grätzel, M. TiO₂ pore-filling and its effect on the efficiency of solid-state dye-sensitized solar cells. *Thin Solid Films* **2006**, *500*, 296–301. [[CrossRef](#)]
28. Kaushik, D.K.; Selvaraj, M.; Ramu, S.; Subrahmanyam, A. Thermal evaporated Copper Iodide (CuI) thin films: A note on the disorder evaluated through the temperature dependent electrical properties. *Sol. Energy Mater. Sol. Cells* **2017**, *165*, 52–58. [[CrossRef](#)]
29. Cao, G.; Huang, F.; Tian, J.; Siffalovic, P.; Li, M. From scalable solution fabrication of perovskite films towards commercialization of solar cells. *Energy Environ. Sci.* **2018**.
30. Nazari, P.; Ansari, F.; Abdollahi Nejand, B.; Ahmadi, V.; Payandeh, M.; Salavati-Niasari, M. Physicochemical Interface Engineering of CuI/Cu as Advanced Potential Hole-Transporting Materials/Metal Contact Couples in Hysteresis-Free Ultralow-Cost and Large-Area Perovskite Solar Cells. *J. Phys. Chem. C* **2017**, *121*, 21935–21944. [[CrossRef](#)]
31. Thanihachelvan, M.; Sockiah, K.; Balashangar, K.; Ravirajan, P. Cadmium sulfide interface layer for improving the performance of titanium dioxide/poly (3-hexylthiophene) solar cells by extending the spectral response. *J. Mater. Sci. Mater. Electron.* **2015**, *26*, 3558–3563. [[CrossRef](#)]

32. Loheeswaran, S.; Balashangar, K.; Jevirshan, J.; Ravirajan, P. Controlling Recombination Kinetics of Hybrid Nanocrystalline Titanium Dioxide/Polymer Solar Cells by Inserting an Alumina Layer at the Interface. *J. Nanoelectron. Optoelectron.* **2013**, *8*, 484–488. [[CrossRef](#)]
33. Loheeswaran, S.; Thanishaichelvan, M.; Ravirajan, P.; Nelson, J. Controlling recombination kinetics of hybrid poly-3-hexylthiophene (P3HT)/titanium dioxide solar cells by self-assembled monolayers. *J. Mater. Sci. Mater. Electron.* **2017**, *28*, 4732–4737. [[CrossRef](#)]
34. Balashangar, K.; Paranthaman, S.; Thanishaichelvan, M.; Amalraj, P.A.; Velauthapillai, D.; Ravirajan, P. Multi-walled carbon nanotube incorporated nanoporous titanium dioxide electrodes for hybrid polymer solar cells. *Mater. Lett.* **2018**, *219*, 265–268. [[CrossRef](#)]
35. Cojocar, L.; Uchida, S.; Jayaweera, P.V.V.; Kaneko, S.; Wang, H.; Nakazaki, J.; Kubo, T.; Segawa, H. Effect of TiO₂ Surface Treatment on the Current–Voltage Hysteresis of Planar-Structure Perovskite Solar Cells Prepared on Rough and Flat Fluorine-Doped Tin Oxide Substrates. *Energy Technol.* **2017**, *5*, 1762–1766. [[CrossRef](#)]
36. Zhu, B.L.; Zhao, X.Z. Transparent conductive CuI thin films prepared by pulsed laser deposition. *Phys. Status Solidi Appl. Mater. Sci.* **2011**, *208*, 91–96. [[CrossRef](#)]
37. Yue, S.; Gu, M.; Liu, X.; Zhang, J.; Huang, S.; Liu, B.; Ni, C. Effect of ZnI₂ cosolute on quality and performance of γ -CuI ultrafast scintillation crystal grown via evaporation method in acetonitrile solvent. *Opt. Mater. (Amst.)* **2017**, *66*, 308–313. [[CrossRef](#)]
38. Madhavan, V.; Ali, A.; Baloch, B.; Manekathodi, A.; Zimmermann, I.; Roldán-carmona, C.; Grancini, G.; Buffiere, M.; Nazeeruddin, M.K.; Belaidi, A.; et al. CuI and CuSCN as Hole Transport Materials for Perovskite Solar Cells. In *Qatar Foundation Annual Research Conference Proceedings Volume 2018 Issue 1*; Hamad bin Khalifa University Press (HBKU Press): Doha, Qatar, 2018.
39. Liu, M.; Endo, M.; Shimazaki, A.; Wakamiya, A.; Tachibana, Y. Identifying an Optimum Perovskite Solar Cell Structure by Kinetic Analysis: Planar, Mesoporous Based, or Extremely Thin Absorber Structure. *ACS Appl. Energy Mater.* **2018**, *1*, 3722–3732. [[CrossRef](#)]
40. Jeon, N.J.; Lee, J.; Noh, J.H.; Nazeeruddin, M.K.; Grätzel, M.; Seok, S.I. Efficient inorganic-organic hybrid perovskite solar cells based on pyrene arylamine derivatives as hole-transporting materials. *J. Am. Chem. Soc.* **2013**, *135*, 19087–19090. [[CrossRef](#)]
41. Zhu, X.D.; Ma, X.J.; Wang, Y.K.; Li, Y.; Gao, C.H.; Wang, Z.K.; Jiang, Z.Q.; Liao, L.S. Hole-Transporting Materials Incorporating Carbazole into Spiro-Core for Highly Efficient Perovskite Solar Cells. *Adv. Funct. Mater.* **2019**, *29*, 1–8. [[CrossRef](#)]
42. Ke, W.; Fang, G.; Wang, J.; Qin, P.; Tao, H.; Lei, H.; Liu, Q.; Dai, X.; Zhao, X. Perovskite solar cell with an efficient TiO₂ compact film. *ACS Appl. Mater. Interfaces* **2014**, *6*, 15959–15965. [[CrossRef](#)] [[PubMed](#)]
43. Nouri, E.; Mohammadi, M.R.; Lianos, P. Inverted perovskite solar cells based on lithium-functionalized graphene oxide as an electron-transporting layer. *Chem. Commun.* **2017**, *53*, 1630–1633. [[CrossRef](#)] [[PubMed](#)]
44. Chen, W.Y.; Deng, L.L.; Dai, S.M.; Wang, X.; Tian, C.B.; Zhan, X.X.; Xie, S.Y.; Huang, R.B.; Zheng, L.S. Low-cost solution-processed copper iodide as an alternative to PEDOT:PSS hole transport layer for efficient and stable inverted planar heterojunction perovskite solar cells. *J. Mater. Chem. A* **2015**, *3*, 19353–19359. [[CrossRef](#)]
45. Li, Z.; Chen, J.; Li, H.; Zhang, Q.; Chen, Z.; Zheng, X.; Fang, G.; Wang, H.; Hao, Y. A facile synthesized “spiro” hole-transporting material based on spiro[3.3]heptane-2,6-dispirofluorene for efficient planar perovskite solar cells. *RSC Adv.* **2017**, *7*, 41903–41908. [[CrossRef](#)]
46. Gheno, A.; Vedraïne, S.; Ratier, B.; Bouclé, J. π -Conjugated Materials as the Hole-Transporting Layer in Perovskite Solar Cells. *Metals* **2016**, *6*, 21. [[CrossRef](#)]
47. Yang, L.; Barrows, A.T.; Lidzey, D.G. Perovskite solar cells with CuI inorganic hole conductor of Ti thin film solvent annealing treatment method. *Jpn. J. Appl. Phys.* **2017**, *56*, 08MC04.
48. Karuppachamy, S.; Murugadoss, G.; Ramachandran, K.; Saxena, V.; Thangamuthu, R. Inorganic based hole transport materials for perovskite solar cells. *J. Mater. Sci. Mater. Electron.* **2018**, *29*, 8847–8853. [[CrossRef](#)]

